Lock-in Detection and Hall effect

Jaewon Jung[1]
[1] *Department of Physics and Astronomy, Seoul National University, Seoul 08858 Korea*
(Received 18 April 2024; revised 20 April 2024; accepted 24 April 2024; published 25 April)

The lock-in detection, a crucial technique that is essential in electronics measurement, is employed to measure the small Hall voltage in an extremely noisy environment. Initially, we measure and calibrate all components of the lock-in amplifier to determine the operational ranges of each component. Subsequently, we measure the magnetic field of the two cylindrical neodymium magnets in three different axes using the Hall sensor along with the lock-in technique. The magnetic moment of the magnets is calculated considering the cylindrical geometry of the magnet, yielding values of 0.148 ± 0.008 A$\cdot$m^2 and 0.127 ± 0.015 A$\cdot$m^2 in the horizontal and the vertical axes, respectively.

I. INTRODUCTION

In this report, we measure a magnetic field from two cylindrical neodymium magnets using GaAs Hall sensor with lock-in amplifier. To do so, we first check the frequency response and the operation behavior of all the components in the lock-in amplifier to find an adequate ranges of parameters of the lock-in amplifier. Next, we utilize the noise generator to test how effectively the lock-in amplifier wipes off the noise from signal particularly under low signal-to-noise ratio. Leveraging the results and observations from prior experiments, we measure the magnetic field induced from two cylindrical neodymium magnets under three different axes using a Hall sensor with a well-calibrated lock-in amplifier and calculated the magnetic dipole moment as well. Notably, all the measurements are automated by low-level control of the oscilloscope using Python which results in a significant reduction of standard deviations and total measurement time compared to the traditional measurement technique which is typically done by reading the oscilloscope by human eyes.

A. Noise figure and Friis formula

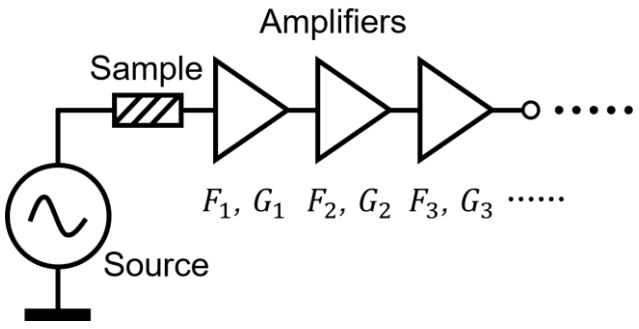

FIG. 1. Schematic of the amplifier chain with each noise factor *F* and the gain *G*.

When multiple amplifiers are used in the circuit, it is important to take in account how the serial amplifiers amplify the noise. Noise figures and gains of each amplifier determine the total noise factor of the amplifier chain as depicted in FIG.1. Noise factor (F) and noise figure (NF) are defined as [1]

$$F = \frac{SNR_{input}}{SNR_{output}}, \qquad NF = 10\log_{10} F, \qquad (1)$$

where SNR is signal-to-noise ratio and NF is in units of decibels (dB). The total noise factor in the amplifier chain is found by Friis formula as below.

$$F_{total} = F_1 + \frac{F_2 - 1}{G_1} + \frac{F_3 - 1}{G_1 G_2} + \cdots + \frac{F_n - 1}{G_1 G_2 \cdots G_{n-1}}, \quad (2)$$

where F_n and G_n are the noise factor and gain for the n-th amplifier

B. Principle of lock-in detection

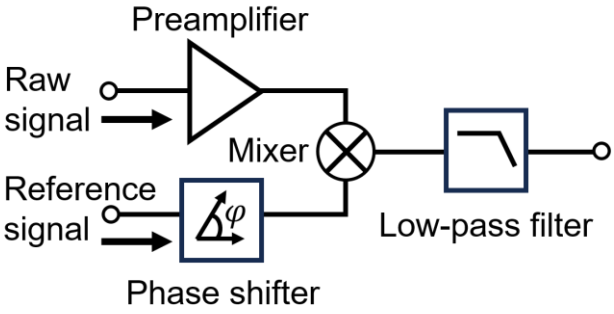

FIG. 2. Basic components of the lock-in detection.

Lock-in detection is a widely used technique that is capable of extracting a known signal at a certain reference frequency and phase from a highly noisy

environment. It is based on the orthogonality of sine waves. Raw signal and the reference sinusoidal signal are multiplied by a mixer and passed to a low-pass filter where the mixed signal is time-averaged which results in DC current if the raw signal contains AC signal of frequency as same as reference signal's frequency. Since the time-averaged results depend on the relative phase between the signal of interest and the reference signal, the reference signal is passed to the phase shifter prior to the mixer to to match the relative phase. A preamplifier with high gain is used at first to amplify the small signal and to reduce the total noise which can be amplified throughout the whole stages of lock-in amplifier according to the Friis formula. From the below calculation, it is straightforward to understand that the lock-in detection gives DC signal if two are in phase.

$$\int 2sin(f_1 t) \times sin(f_2 t + \varphi) dt$$
$$= \int (\cos((f_1 - f_2)\, t - \varphi) - \cos\big((f_1 + f_2)t + \varphi\big)\, dt$$
$$\approx cos\varphi, \quad if\ f_1 = f_2\,, \qquad (3)$$

where φ is a relative phase.

C. Double Balanced Mixer (DBM)

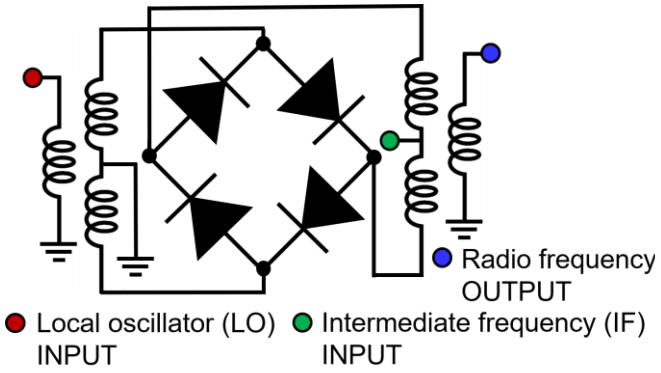

FIG. 3. Circuit diagram of double balanced mixer.

The double balanced mixer (DBM) is used instead of actual multiplication of raw signal and reference signal in the lock-in detection process in this experiment. Double balanced mixer has two input signals and outputs one of the input signals multiplied by the sign of the other input signal. It is also known to have good isolation of LO-RF and LO-IF that leads to broadband response which is favorable for lock-in experiments.

D. Low-pass filter

Low-pass amplifier is also an essential component in lock-in amplifier. In principle, low-pass filter is a filter that filters out the frequencies which are above cutoff frequency. From the multiplied two sinusoidal functions in Eq. 3, the high frequency part can be filtered out when it is passed to the low-pass filter. As a result, the low-pass filter works like an integrator. The low-pass filter we use is an RC circuit that is tunable by adjusting the time constant and the roll-off. The time constant is the time required to charge the capacitor which determines the cutoff frequency of the low-pass filter. The roll-off is the rate of attenuation of the gain around the cutoff frequency which determines the bandwidth of the low-pass filter. The quality factor (Q) means how sharp the filter's response is around the cutoff frequency, therefore, if the roll-off is large, the Q factor is also high which leads to narrow bandwidth increasing the sensitivity of the lock-in amplifier.

E. Hall effect

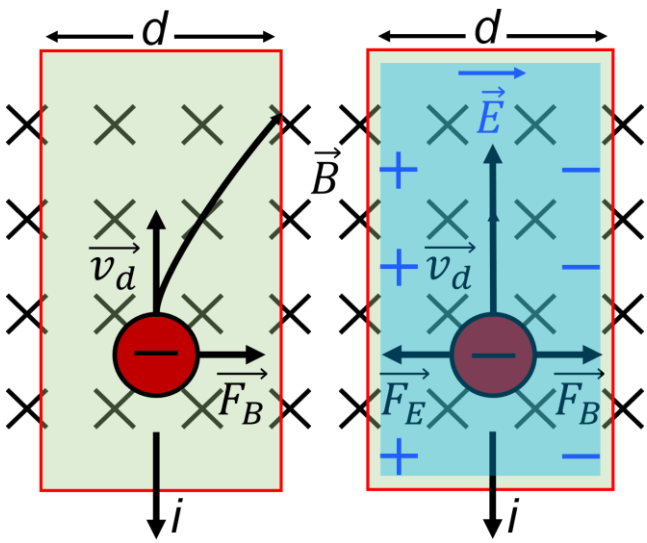

FIG. 4. Hall effect on moving charge in a uniform magnetic field. Left: the negative charge carrier initially enters the magnetic field and gets Lorentz force which deviates its moving direction. Right: in a steady state, the charge carriers are cumulated to the right side until the electric force and the Lorentz force are in equilibrium.

When an electric current passes through a conductor in a magnetic field the charge carriers get Lorentz force due to the magnetic field which leads to potential difference across the conductor. The potential difference here is defined as Hall voltage and the corresponding equations are as follows

$$eE = evB, \qquad i = -nevA$$
$$V_{Hall} = Ed = -R_H iB\frac{d}{A}\,, \qquad (4)$$

where, the Hall coefficient $R_H = 1/ne$, d and A are the width and the cross section of the conductor and n is the carrier density. Since we know the current, d and A from Eq. 4, we can measure the magnetic field directly by measuring the Hall voltage.

F. Magnetic dipole moment

Since there is no magnetic monopole, any system that has a net magnetic field possesses a dipole moment with the higher-order multipole moments. The magnetic field then defined by [3]

$$\vec{B} = \frac{\mu_0}{4\pi}\frac{3(\vec{m}\cdot\hat{r})\hat{r} - \vec{m}}{r^3}, \qquad (5)$$

where, $\vec{m}$ is a dipole moment and $\hat{r}$ is unit vector in its direction. Although there exist multipole components in real magnets, those vanish rapidly as the distance increases ensuring the dipole approximation is valid in the practical regime.

G. Kramers-Kronig relation

The Kramers-Kronig relation, or Sokhotski-Plemelj theorem in mathematical area, is the relation that links the real and imaginary parts of a complex function that is analytic in the upper half-plane. The relation is defined by [3]

$$\begin{aligned} G(\omega) &= G_1(\omega) + iG_2(\omega) \\ G_1(\omega) &= \frac{1}{\pi}P\int_{-\infty}^{\infty}\frac{G_2(\omega')}{\omega' - \omega}d\omega' \\ G_2(\omega) &= -\frac{1}{\pi}P\int_{-\infty}^{\infty}\frac{G_1(\omega')}{\omega' - \omega}d\omega', \end{aligned} \qquad (6)$$

where, ω is a real number and P represents the Cauchy principal value. In this experiment, we measure frequency response of a preamplifier and a low-pass filter which then can be analyzed by above relation from the measured real values.

II. METHODS

In this experimental setup, TeachSpin's Signal Processor/Lock-In Amplifier is utilized and the Protek GD-0020N DDS Function generator and Rigol DHO924S oscilloscope are used for generating reference signal and measuring the signals. All the connections between devices are done by BNC cables with BNC tee for multiple inputs or outputs. For Hall effect experiment, the MG910 GaAs Hall sensor with the integrated Hall mount is used. All the measurements conducted with the oscilloscope are performed by low-level control via Python. This approach enables fast and accurate measurements and also the direct access to the raw data.

A. Calibration and sanity check of the Signal Processor/Lock-In Amplifier

In the lock-in detection procedure, the key components are a preamplifier, a phase shifter, a double balanced mixer, and a low-pass amplifier. For accurate lock-in detection in the Hall voltage measurement, it is crucial to examine the limit and the operational boundaries of each component. Therefore, we observe the frequency response of the preamplifier, phase shifter, and low-pass amplifier and verify if the mixer works as desired.

A.1 Frequency response of the preamplifier

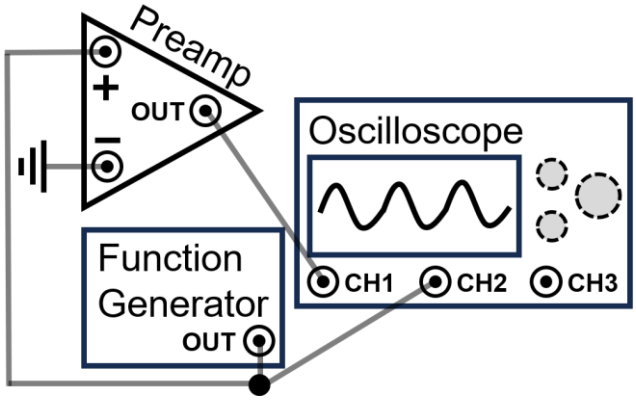

FIG.5. Experiment setup for measuring preamplifier's frequency response.

The preamplifier serves as the initial stage where the signal passes through. To determine the operational range within which the preamplifier amplifies the signal by the specified gain, we measure the frequency response of the preamplifier's gain. For gains 1, 2, 5, 10, and 20, we send a sinusoidal signal ranging from 1 kHz to 14.5 MHz with the fixed amplitude of 100 mV and measured the gain of the amplitude of the output sinusoidal signal. We measure 1000 samples from the oscilloscope within the appropriate time window for each frequency and calculated gain by fitting the input signal and the output signal to the sinusoidal function. We also calculated the frequency of the input and output signal to account for the deviation of the set frequency of the function generator and the actual signal. From the measurement result, we determine the 3dB frequency by a linear regression.

A.2 Frequency response and calibration of the phase shifter

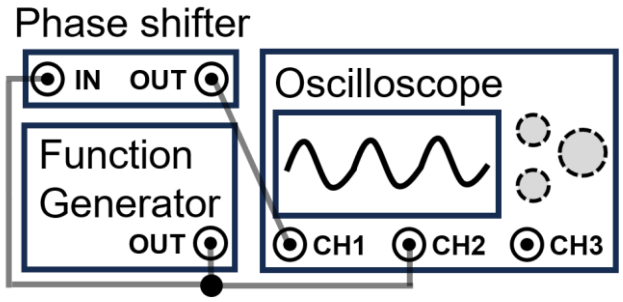

FIG. 6. Experiment setup for measuring the frequency response and calibrating the phase shifter.

In the same manner, the phase shifter works properly in the appropriate frequency range, which is specified by 3 Hz through 3 kHz in the specification. For phase shift of $30°, 120°$, we send a sinusoidal signal ranging from 23.5 Hz through 1.95 MHz with the same fixed amplitude of 100 mV and measured the phase shift of the output signal compared to the input phase shift. From the observation in this experiment, we chose 1 kHz signal and measured the phase shift of the output signal compared to the input phase shift while setting the input phase shift from 0° to 330° in increments of 30° to verify if the phase shifter shifts the phase of input signal as intended.

A.3 Sanity check of double balanced mixer

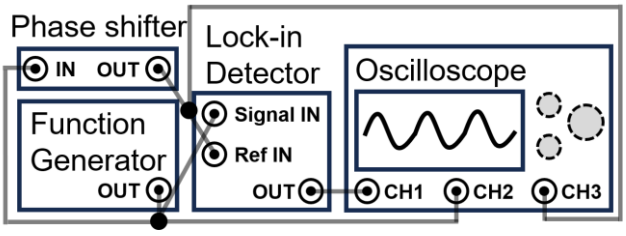

FIG. 7. Experiment setup for observing the behavior of double balanced mixer.

Using the phase shifter and the double balanced mixer together, we send a 1 kHz, 100 mV signal to the phase shifter and the mixer varying the phase shift of $0°. 45°, 90°, 135°, 180°,$ and $270°$. We then observe the input signal and the phase shifted signal together to verify if they are in phase or out of phase as we set and observed the resulting mixed signal from the other channel. From the input signal and the phase-shifted signal, we fit the two sinusoidal signals to accurately match the phase and fine-tune the phase shifter from the feedback of fitted results.

A.4 Frequency response of a low-pass amplifier

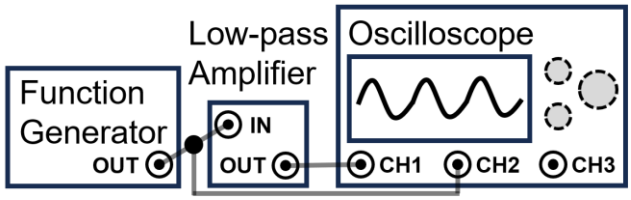

FIG. 8. Experiment setup for measuring the frequency response of the low-pass filter.

It is viable to tune the cutoff frequency and the Q factor of the low-pass filter by setting the time constant and the roll-off of the filter. We choose the time constant of 0.03, 0.3, 0.1, and the roll-off of 6 and 12, and from the possible 6 combinations, we measure the frequency response of the low-pass filter. We send a sinusoidal signal ranging from 0.01 Hz to 1 kHz with a fixed amplitude of 100 mV and measured the gain of the output signal compared to the input signal. The gain is calculated from the fitting result as same as A.1.

B. Lock-in detection

After the calibration and sanity checks are done, we now test the performance of the lock-in amplifier by measuring the signal under a tunable artificial noise source. We first analyze the spectrum of signal with noise and then conduct lock-in detection to see if the lock-in amplifier can safely extract the signal even under a poor signal-to-noise ratio. The DC offset stability of the lock-in amplifier is assessed by generating the DC offset to the noise and see if the output gain varies with the DC offset or not.

B.1 Spectrum analysis of the signal with noise

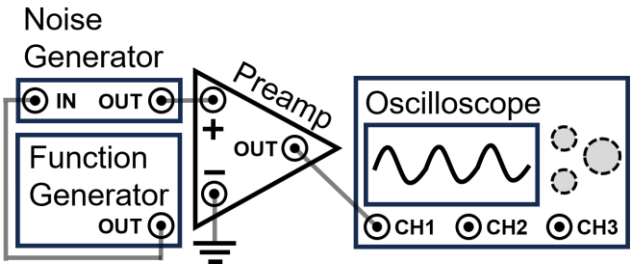

FIG. 9. Experimental setup for analyzing the Fast Fourier Transform (FFT) spectrum of signal with artificial noise.

We use a signal of 1 kHz and 100 mV amplitude and vary the noise amplitude as 0, 0.0001, 0.001, and 0.1, where the noise amplitude is normalized as 1 V. We measure the time domain signal from the oscilloscope and perform FFT to see if the reference signal's frequency is well separated from the noise frequencies in the frequency domain.

B.2 Lock-in detection of the signal under noise

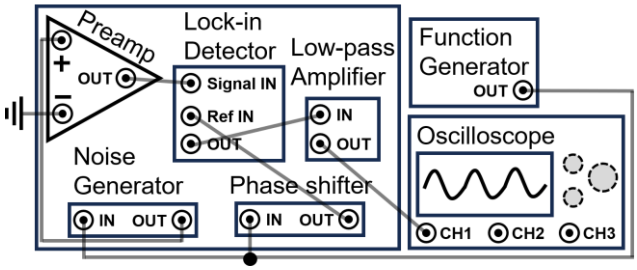

FIG. 10. Experiment setup for conducting the lock-in detection under artificial noise.

For the preamplifier, we use the gain 10 and set the DC/AC switch of the preamplifier to AC and set the phase shift value to the one that maximizes the output signal of the lock-in amplifier. For the low-pass amplifier, the time constant of 0.3 and the roll-off of 6 is used and the gain of the filter is set to 1 since filter's gain is not tested. For the noise generator, amplitude of 0, 0.0001, 0.001, and 0.1 are used. Under above conditions, we measure the gain of the DC output varying the phase shift to find the phase that maximizes the gain. The phase shifts and gains are measured by fitting the raw data from the oscilloscope. The resulting gain versus phase data are then fitted to the cosine function as derived in Eq. 3.

B.3 DC offset stability of lock-in detection

From the same experimental setup in B.2, break the function generator's output and connect the two BNC cables to the preamplifier and the noise generator with the DC offset added to the function generator. By differing the offset percentile from 0 % to 100% in increments of 5 %, measure the gain of the DC output signal compared to the input signal.

C. Hall effect based magnetic field measurement with lock-in detection

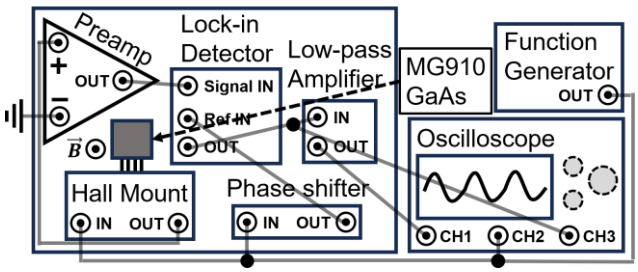

FIG. 11. Experiment setup for the Hall effect experiment.

The MG910 GaAs Hall sensor is known to induce around 45 mV under the magnetic field of 50 mT with 5 mA current at room temperature. Thus, we use the same parameters of the lock-in amplifier and the function generator in B.2 and connect the Hall sensor instead of the noise generator for now. To accurately measure the magnetic field in three different axes we built a measurement setup that can tightly hold the position of the Hall sensor and vary the magnet's position to change the distance between the sensor and the magnet as in FIG. 12.

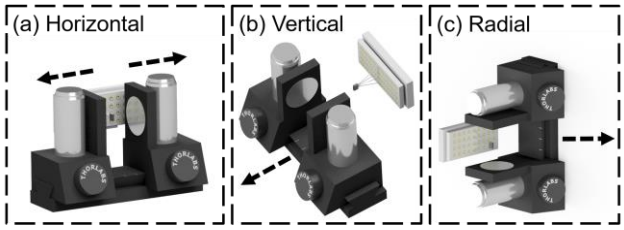

FIG. 12. Three axes measurement setup. The arrow indicates the direction of the magnet's movement. The Hall mount is fixed vertically at the wall.

III. RESULTS

All the measurements are done with high accuracy owing to the Python based raw data measurement that the standard deviation in the most of the data are not visible. Therefore, unless it is specified, the standard deviation is omitted in the results.

A. Frequency response of the preamplifier

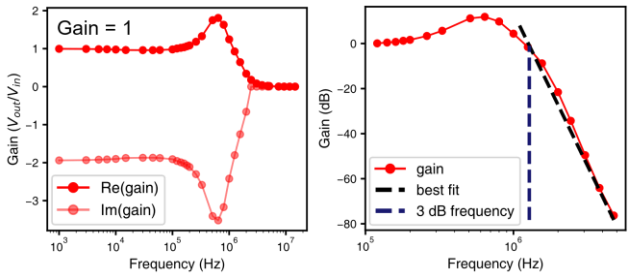

FIG. 13. Frequency response of the preamplifier at gain 1. The imaginary part of the gain is obtained from the Kramers-Kronig relation.

From the FIG. 13-14, it is found that the gain (dB) of the preamplifier decreases linearly as the frequency increases. Here, the gain in dB unit is defined as $20\log(V_{out}/V_{in})$, therefore, the linear fit is done using the equation $a\log f + b$ and the roll-off can be defined by $|a|log2$, where, a and b are the coefficient and f is the frequency. In particular, as the pre-selected gain value increases from 1 to 20, the corresponding 3 dB frequency also gets smaller and the peak of the gain decreases. This behavior is apparent in the imaginary part of the gain as well while the roll-off remains around 40 dB/oct across the different gains.

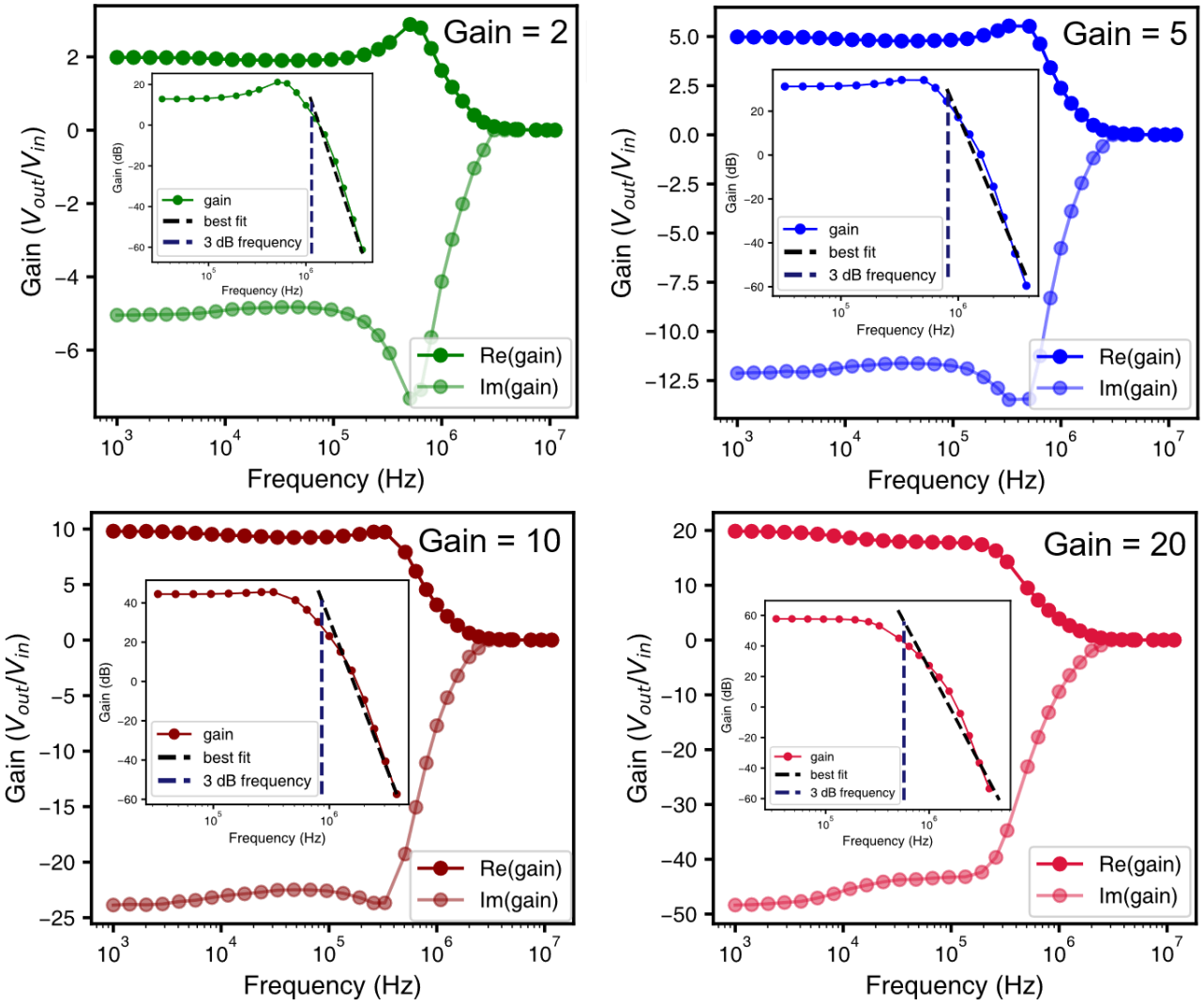

FIG. 14. Frequency response of the preamplifier at gain 2, 5, 10, and 20. The imaginary part of the gain is obtained from the Kramers-Kronig relation.

TABLE I. The measured 3 dB frequency and roll-off value for each gain in FIG. 13-14. The uncertainties are calculated by using the error propagation technique.

Gain	3 dB frequency	Roll-off
1	1280±1.74 kHz	49.79±2.37 dB/oct
2	1145±1.85 kHz	42.95±2.53 dB/oct
5	868±5.74 kHz	38.04±4.27 dB/oct
10	851±1.51 kHz	46.05±2.10 dB/oct
20	571±1.78 kHz	38.24±2.49 dB/oct

B. Frequency response of the phase shifter

From the frequency response result of the phase shifter, it is observed that the output phase shift depends linearly on the frequency in log scale below 3 kHz which is the specified upper limit of the operational frequency in the specification sheet. Beyond this limit, the measured phase shift tends to increase slowly for a moment and the increase linearly again with the steeper slope. Under the upper limit frequency, the 1 kHz signal showed accurate phase shift output from the phase shifter as seen in FIG. 15 which is consistent with the frequency response result indicating the 1 kHz signal is safe to use on the phase shifter.

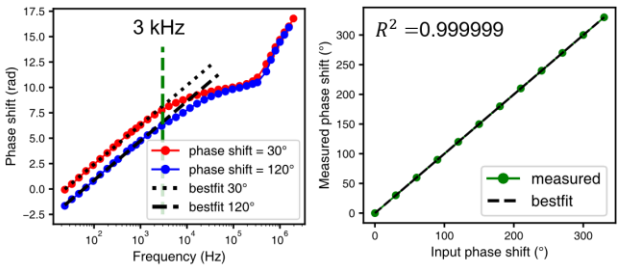

FIG. 15. Frequency response and the phase shift response of the phase shifter. The phase response is measured using 1 kHz sinusoidal signal and fitted to the linear function with R^2= 0.999999

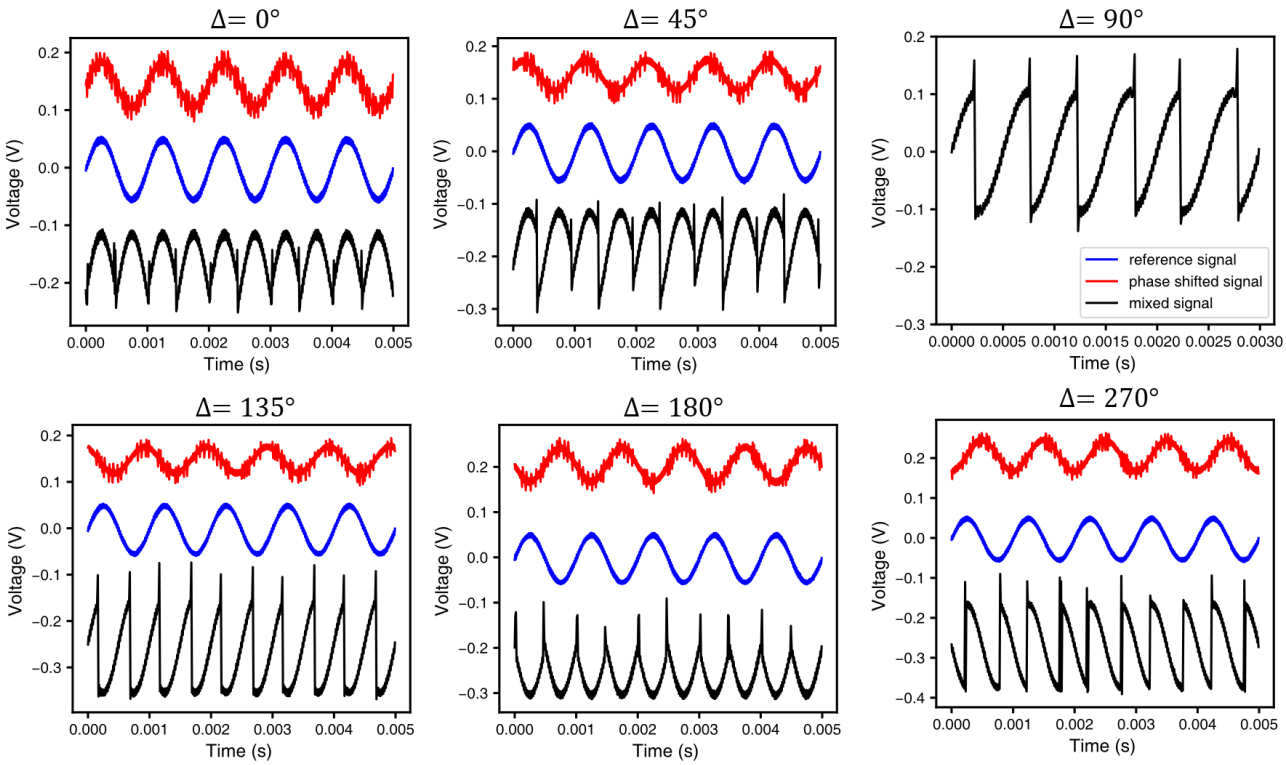

FIG. 16. The result of the double balanced mixer. Δ denotes the phase shift and the red, blue, and black signals represent the phase-shifted, reference, and the mixed signal. The signals are plotted with an adequate amount of offset.

C. Mixing of the double balanced mixer

In FIG. 16, it is observed that the double balanced mixer outputs the mixed signal of the reference input and the sign of the phase-shifted signal. Note that, while the reference signal has low noise, the phase-shifted signal shows high-frequency noise that consequently introduces noise to the mixed signal. This type of noise can be easily filtered. For example, using the Butterworth filter, the filtered signal has almost the original 1 kHz part as can be both seen in the time domain and the frequency domain in FIG. 17. However, since we are not using the filter in this experiment, this noise is kept throughout the rest experiment.

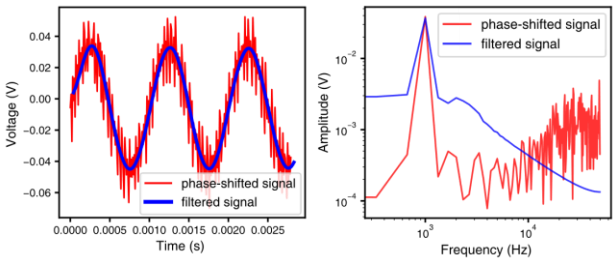

FIG. 17. Left: The phase-shifted signal (red) from FIG. 16 and the filtered signal using Butterworth signal (blue). Right: Fast Fourier Transform (FFT) results of the signals in the left graph.

D. Frequency response of the low-pass filter

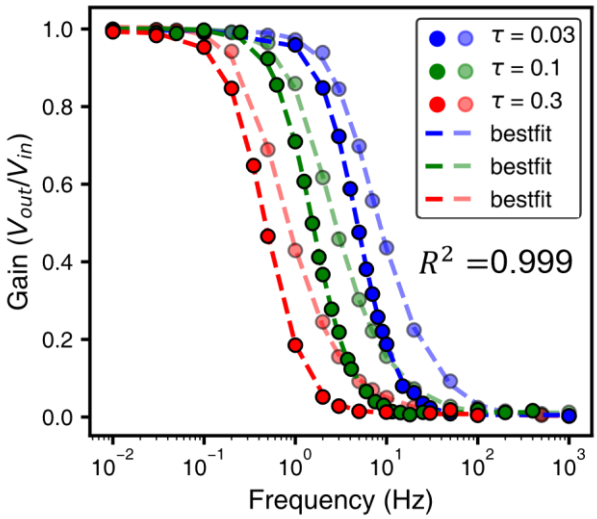

FIG. 18. The frequency response of the low-pass filter for different time constants and roll-off settings. The transparent dots and dashed lines are the ones with a roll-off is 6 and the others are the ones with a roll-off of 12. R^2 values for all 6 combinations exceed 0.999.

The frequency response results are consistent with the theoretical predictions that for the fixed roll-off, as the time constants increase, the cutoff frequency decreases. For the fixed time constants, as the roll-off increases from 6 to 12, the gain decreases from 1 to 0 much faster. The different fitting functions are

used as in Eq. 7 for the roll-off of 6 and 12 since the roll-off of 6 is 1st-order low-pass filter while the roll-off of 12 is 2nd-order low-pass filter.

$$Gain_{1st} = \frac{1}{\sqrt{1+(2\pi f\tau)^2}},$$
$$Gain_{2nd} = (Gain_{1st})^2 = \frac{1}{1+(2\pi f\tau)^2} \qquad (7)$$

where, f, τ are the frequency, and the time constant.

E. Spectrum of signal with white noise

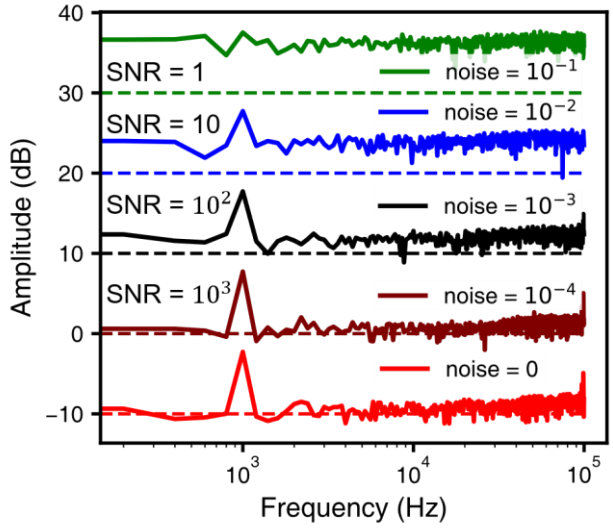

FIG. 19. The noise spectrum of a 1 kHz signal with different noise amplitudes Noise spectrums are plotted with an offset and the dashed lines indicates the baselines for each spectrum. The signal-to-noise ratios (SNR) are calculated from the input signal amplitude of 100 mV and the noise amplitude which has a maximum 1 V_{rms}. The horizontal lines are offset by 10 dB.

In FIG. 19, as the noise amplitude increases, noises are added to all frequency areas, while the noise seems to be more random for the high-frequency range. The signal at 1 kHz is almost indistinguishable when the SNR is 1 at the noise amplitude of 10^{-1}. Even without the noise generator, we can see that there is plenty of noise in high-frequency areas but the 1 kHz seems to be a safe frequency away from this background noise.

F. Lock-in detection of signal

The results in FIG. 20 show that the output of the lock-in amplifier depends on the phase sinusoidally. When the SNR is 1, the lock-in amplifier still gives the same output compared to when there is no additional noise other than the background noise. This suggests that if the frequency of the signal of interest is well separated from the noise, it is still possible to measure it even with the extremely low SNR. The bias between the measured result and the fitted results are mostly from the miscalibration of the phases since all the results are consistent with each other.

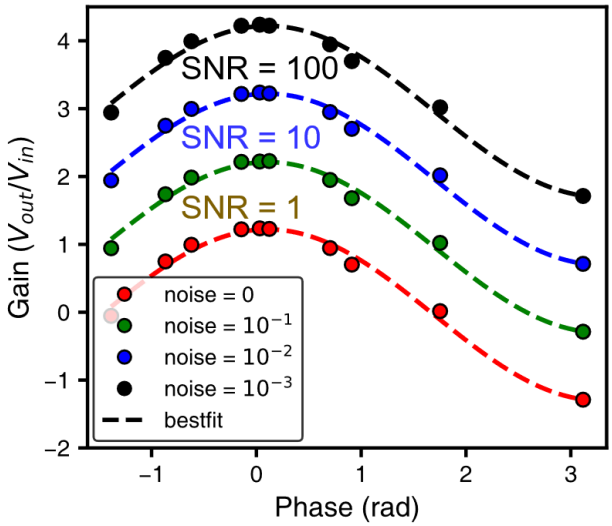

FIG. 20. The phase dependence of the gain from lock-in amplifier with different signal-noise-to ratio (SNR). The dashed lines represent the cosine fit results. R^2 values are all the same as 0.987. The SNRs are drawn with an offset by a gain of 1.

G. DC offset stability of a lock-in detection

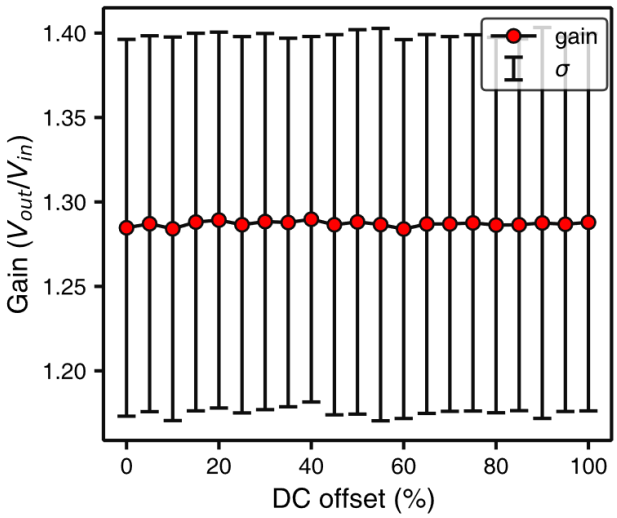

FIG. 21. The gain of the lock-in amplifier with different DC offsets in the input signal. σ represents the standard deviation.

The DC offset is known for not affecting the lock-in amplifier result and the result in FIG. 21 is consistent with this fact. So far, the measurements

are done multiple times to reduce the standard deviation and increase the accuracy, here, on the other hand, measurements are done with a single measurement to find out the noise figures of the whole chain of our lock-in amplifier. The detailed calculation of the noise factors using the Friis formula is dealt in the discussion section.

H. Measurement of a magnetic field produced by a pair of neodymium magnets using a Hall magnetometer with the lock-in amplifier

Prior to measuring the Hall voltage from the magnets, we checked if the signal and the reference signal are in phase and verified that the output Hall voltage has a linear relationship between the input voltage as shown in FIG. 22.

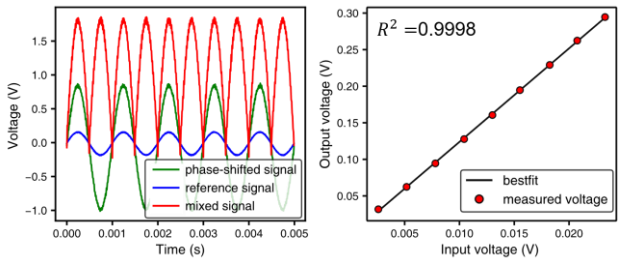

FIG. 22. The in phase of reference signal and the phase-shifted signal (left) and the linear relationship between the input voltage with the Hall voltage (right).

For the Hall voltage measurement, we measured 100 times per data points to be more accurate since the Hall voltage is very weak signal compared to the ones we measured before. The standard deviation of measured Hall voltage is smaller than the Hall voltage in the order of $10^{-3} \sim 10^{-4}$ that the measurement was accurate but due to the uncertainty in the resistance and the Hall coefficient of the Hall sensor, the measured magnetic field has a large standard deviation compared to the Hall voltage. To compensate for the background current in the absence of a magnetic field, we subtract this background voltage from the measured Hall voltage. The magnetic field and corresponding uncertainty is calculated by following equation.

$$B = 50\ \text{mT} \times 5\ mA \times \frac{R}{V_i} \times \frac{V_m - V_{back}}{V_H},$$

$$\sigma = \sqrt{\sum_i \left(\frac{\sigma_{O_i}}{O_i}\right)^2} \qquad (8)$$

where, V_m, V_{back}, and V_i represents measured Hall voltage, background voltage and the input voltage. V_H and R represents the Hall voltage and the resistance of the MG910 GaAs Hall sensor in room temperature [4]. The 50 mT and 5 mA is the magnetic field and current at room temperature which are our reference values. O_i denotes each observable used in B field equation. The corresponding values of observables and standard deviations are listed in Table II. The standard deviation for V_H and R is calculated assuming the minimum and maximum of each value as the 95 % confidence level.

TABLE II. The measured values and standard deviations.

	Values	σ
V_H	45 mV	5.5 mV
V_{back}	1.1514 mV	0.022 mV
V_i	108.19 mV	1.07×10^{-5} mV
R	750 Ω	61 Ω

Here, the magnetic fields are fitted using the dipole approximation. For the vertical axis, the dipole approximation gives the answer close to the experimental data with R^2 of 0.944 while horizontal axis result cannot be explained using the dipole moment only. It's due to the fact that the magnetic field induced from the dipole moment decreases in the order of r^{-3} while there exist more contributions other than the dipole term. The minus magnetic field comes from the background noise in the order of 1 mV. The radial axis result in FIG. 24 shows close to the zero magnetic field considering the uncertainty in the magnetic field, which is consistent with the theory that there is no magnetic field at the radial axis of the magnet. Considering the geometry of the real magnet is discussed in the discuss section.

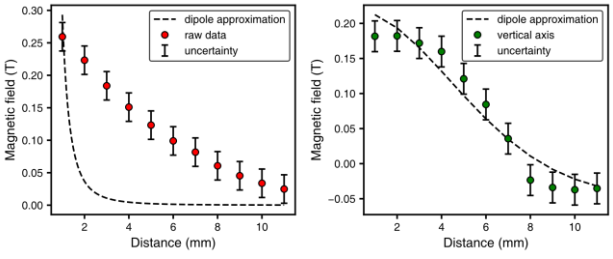

FIG. 23. The magnetic field measured at the horizontal and the vertical axis. The two are fitted using the dipole approximation. R^2 value for the vertical fit is 0.944 and the magnetic moment is calculated as 0.181±0.028 A· m^2 from the vertical result.

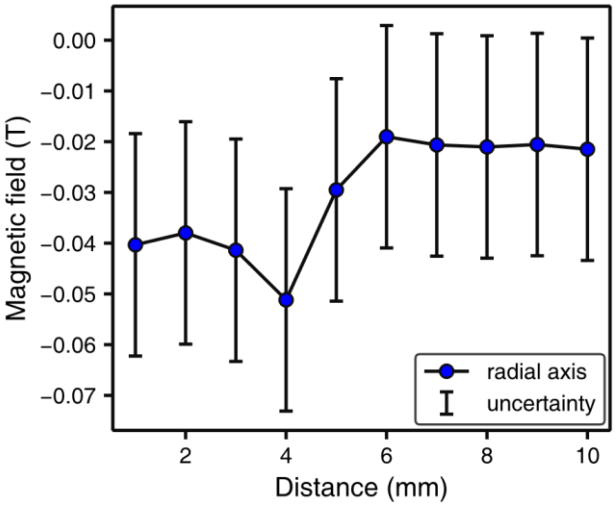

FIG. 24. Magnetic field in the radial axis of the Hall sensor. σ represents the standard deviation.

IV. DISCUSSIONS

A. The noise factor of the lock-in amplifier

From the Friis formula, the total noise factor is sum of the noise factor with dividing the stage gains. Since we only use a gain of 10 from the preamplifier at the first stage, the sequential noise factors in the summation only decrease by 10, therefore, the noise factors from after the preamplifiers still possibly contribute to the total noise factor. From the specification sheet, the noise value is specified for the preamplifier and it has a noise of 9 nV/Hz$^{1/2}$ at 1 kHz. In FIG. 21, the noise floor is approximately 10 mV and the noise from the preamplifier is 0.00028 mV which is relatively smaller than the total noise. Considering that the combined noise from both the lock-in and the low-pass filter is lower than the noise from the preamplifier, it is evident that the predominant source of noise cannot be from the amplifier chains. As observed in FIG. 17, the phase shifter also contributes to the total noise of about 10 mV, which is about the same order as the total noise. Thus, the dominant noise source is not from the amplifier chain but from the phase shifter.

B. Multipole contributions in the magnetic field

In the horizontal axis, the dipole moment and the distance vector are parallel so that it is viable to correct the multipole terms easily compared to the vertical axis. The vector field is defined as [3]

$$\vec{A}(\vec{r}) = \frac{\mu_0}{4\pi}\sum_{n=0}^{\infty}\frac{1}{r^n}\int \vec{J}(\vec{r'})\cdot\left|\vec{r'}\right|^n P_n(cos\alpha)d^3r' \,, \quad (7)$$

where, $P_n(cos\alpha)$ is the Legendre polynomial and the α is the angle between r' and r. $\alpha = 0$ in the horizontal axis, therefore, the Legendre polynomial became 1 for all n and resulting magnetic field has the form of summation of $1/r^n$ over n = 0 to infinity up to a constant factor. However, as seen in FIG. 24, the dipole term already falls to the ground rapidly, therefore, additional contributions from the multipole terms are not worth it which indicates that the magnet we use cannot be approximated to the dipole.

C. Magnetic field of the cylindrical magnet

The neodymium magnet has a cylinder-like form so that the magnetic field can be calculated analytically using the boundary conditions of the magnetic field. The magnetic scalar potential is given by triple integral and by applying the boundary conditions in the cylindrical coordinate, radial and the vertical part of the magnetic field is given by [2]

$$B_z = -\frac{\mu_0}{4\pi}M\int_0^{2\pi}\int_0^{a}\left(\frac{R\left(\frac{L}{2}-z\right)}{\left(R^2+\left(\frac{L}{2}-z\right)^2+\rho^2-2R\rho cos\varphi\right)^{\frac{3}{2}}}+\frac{R\left(\frac{L}{2}+z\right)}{\left(R^2+\left(\frac{L}{2}+z\right)^2+\rho^2-2R\rho cos\varphi\right)^{\frac{3}{2}}}\right)dRd\varphi,$$

$$B_\rho = -\frac{\mu_0}{4\pi}M\int_0^{2\pi}\int_0^{a}\left(\frac{R(\rho-Rcos\varphi)}{\left(R^2+\left(\frac{L}{2}-z\right)^2+\rho^2-2R\rho cos\varphi\right)^{\frac{3}{2}}}+\frac{R(\rho-Rcos\varphi)}{\left(R^2+\left(\frac{L}{2}+z\right)^2+\rho^2-2R\rho cos\varphi\right)^{\frac{3}{2}}}\right)dRd\varphi, \quad (8)$$

where, M is a magnetization, a and L are a radius and a height of the magnet. The magnetization and the magnetic moment m have a relationship of $M = m/V$, where V is a volume of the magnet. Using above equation, the magnetic field can be accurately fitted as in FIG. 25.

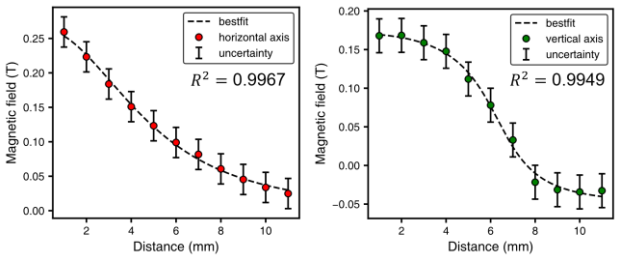

FIG. 25. The magnetic field measured in the horizontal and the vertical axis fitted using Eq. 8. The calculated magnetic moments are 0.148 ± 0.008 A · m^2 (horizontal) and 0.127±0.015 A· m^2 (vertical) where the two results are consistent with each other.

The deviation in the minus magnetic field in the vertical axis result is due to the background noise. It can be further reduced by applying the appropriate filter to the phase shifter which is the main noise source as discussed in A.

V. CONCLUSIONS

Here, we measured the frequency response and the operating behavior of all the components in the lock-in amplifier, such as a preamplifier, a phase shifter, a double balanced mixer, and a low-pass filter. We found that a 1 kHz signal is safe to use for all the components. Using the conditions obtained from them, we measure the magnetic field induced by the two cylindrical neodymium magnets using the GaAs Hall sensor with the lock-in amplifier. The measurement results are consistent with the cylinder model of the magnets and the measured magnetic moments are 0.148 ± 0.008 A$\cdot$ m^2 and 0.127 ± 0.015 A$\cdot$ m^2 for the horizontal and the vertical axis while the magnetic field is measured to be near zero in the radial axis. From the calculation of Friis formula and the measurement results, the major noise source is not from the amplifier chain but from the phase shifter in the order of 10 mV while the total amplifier chain of the lock in detector has noise under 1 μV. The high-frequency noise introduced at the phase shifter can be eliminated effectively using the Butterworth filter that we suggest to use the filter for the accurate measurement when using the lock-in amplifier.

ACKNOWLEDGEMENTS

The author wants to thank our teammates, Juwon Choi, Hyeonsung Jo, and Junyoung Lee for conducting the experiments and having valuable discussions throughout the experiment day. The author also wants to thank T.A. for supporting the initial setup and the maintenance of the lock-in amplifier devices.

REFERENCES

[1] Horowitz, P., & Hill, W. (2015). *The art of electronics* (3rd ed.). Cambridge University Press.
[2] S. M. Blinder "Magnetic Field of a Cylindrical Bar Magnet"
http://demonstrations.wolfram.com/MagneticFieldOfACylindricalBarMagnet/
Wolfram Demonstrations Project
Published: July 26 2011.
[3] D. J. Griffiths, Introduction to Electrodynamics, 4th ed. (Cambridge University Press, Cambridge, 2017).
[4] Matrix Opto Co., Ltd. "*MG910 GaAs Hall Element" (*version 3.3).